International Journal of Signal Processing, Image Processing and Pattern Recognition
Vol.9, No.4 (2016), pp.233-246
http://dx.doi.org/10.14257/ijsip.2016.9.4.22

A New Histogram Based Shape Descriptor in Image Retrieval

Ying Guo and Siquan Yu

School of Information and Control Engineering, Liaoning Shihua University, Fushun China, 113001
guoyingfs@163.com, Siquanyu@126.com

Abstract

A shape based descriptor in image retrieval is proposed in this paper. It is focused on developing soft computing efficiency and novelty in image processing. The algorithm calculates a histogram based on the shape descriptor, representing texture feature of an image at high level (object oriented) effectively. By integrating the algorithms in key point detector with shape descriptor, the new method works fairly well compared with the state-of-the-art performance. The new detector detects relationships among key points, regardless of other pixels. That adds robustness to a large extent. Not only spatial relationships, but also variations in texture information are included in the descriptor as well. Structuring elements' description (SED) and a set of overall texture descriptors in an image (short for TXT) are adopted for comparison. Experiments show that the new method performs the best with the 0.25 higher than the other two methods in robustness and accuracy. The new feature is flexible in multi-situations for different objects of interest.

Keywords*: Harris detector, shape descriptor, texture feature, spatial relationships, image retrieval*

1. Introduction

Efficiency and accuracy are extremely significant in image retrieval, especially for a large database. Moreover, both of them remain problems for the methods proposed up to now. In [4, 9, 19, 23 and 39], content based image retrieval (CBIR) has been widely used for its high subjectivity [25, 29, 37]. It is aiming to retrieve images with similar characteristics to the manually selected typical sample of a category.

Notable advances have been made in image retrieval based on texture features. Mathematical Morphological theory is an active area where various algorithms have been proposed to detect targets. Mura, *et. al.* proposed morphological attribute profiles (APs) based on morphological profiles (MPs) [7-8]. They are both widely used in classifying panchromatic images with very high resolution (VHR) [1, 5, 34]. However, morphological operations, especially based on filters by reconstruction [27], are computational expensive. Inglada proposed to use different geometric features for different targets [15]. But they are largely limited by priori knowledge. Texture measures, such as grey level co-occurrence matrix (GLCM) and geo-statistical functions have been largely developed [16, 24, 30]. These low dimensional features are restricted by the whole distribution of pixels in an image. On the other hand, features like Scale Invariant Feature Transform (SIFT) [18], Local Binary Pattern (LBP) [22], histogram of oriented gradient (HOG) [14], and Structure elements' descriptor (SED) [36] work well for describing either low level (local-oriented) or high level (object-oriented) information. Experiments have shown that SED works better with higher precision and re-call than multi-text histogram (MTH) [21], micro-structure descriptor (MSD) [20] and color-spatial feature (CSD3) [19] using databases of Core-1000 and Core-1000.

ISSN: 2005-4254 IJSIP
Copyright ⓒ 2016 SERSC

As for features describing shape patterns, LBP [3] and HOG [2-28] have been proposed and applied to various aspects. Unfortunately, LBP and HOG are badly influenced by the positions of key points. They both describe the distribution of pixels in the neighborhood of every key point. When the key points are located near to the edges of image, LBP and HOG would fail to work. To avoid such circumstances, a new feature is generated in this paper. It describes relative relationships among key points, rather than that between each key point and its neighboring pixels. Therefore, the new feature would be less influenced by the positions of key points in the image. Two features are appointed as comparative methods. One is SED, a recently proposed texture feature. It describes the shape of all the pixels grouped into the same bin. That is a new idea in performing shapes of pixels in the image. The other is TXT (*e.g.* entropy, variance, mean intensity), widely used for representing the overall distribution of an image. SED and TXT are both good performers for images in terms of texture information. However, experiments show that the new feature achieves higher retrieval *F-measure* than SED and TXT.

The following two parts of this paper describe Harris detector and shape descriptor based on the key points detected by Harris respectively. In Part Four, details of the experimental parameters and results are introduced. Conclusions and discussions are illustrated in Part Five.

2. Harris Corner Detector

Key points used in the newly proposed feature are detected by Harris detector [13]. It is based on the assumption that corners are the pixels with maximum local autocorrelation function [33]. Harris corner detector has been proved to be stable in different time domains [26]. It also plays a key role in detecting features in various projects [6] with a general idea as follows:

(1) Gradients in vertical and horizontal directions of every pixel are calculated respectively and images I_x and I_y are generated accordingly.

(2) A Gaussian kernel with size of 3x3 is adopted to smooth gradient images I_x and I_y. Therefore, we get two smoothed images, $I_{x\_gaussian}$ and $I_{y\_gaussian}$.

(3) Harris matrix A is formulated with the following formula,

$$A = \begin{bmatrix} I_{x\_gaussian}^2 & I_{x\_gaussian} I_{y\_gaussian} \\ I_{x\_gaussian} I_{y\_gaussian} & I_{y\_gaussian}^2 \end{bmatrix} \quad (1)$$

(4) The probability P of every pixel being a key point is calculated by evaluating determinant and trace of matrix A.

$$P = \det(A) - k\,trace^2(A) \quad (2)$$

where k is a tunable parameter to meet different demands, and key points are obtained by setting thresholds of P. In our experiment, k is selected to be 0.04 as recommended in [13]. P is determined to be 180. Details about its determination are introduced in Part Four.

3. Histogram Based Shape Descriptor (HSD)

After detection of key points, a new shape descriptor will describe the relationship among different key points, rather than that described in SIFT, LBP, and HOG. To clarify the new descriptor, an illustration is added in Figure 1. The red pixel is a center key point, and blue points represent neighborhood key points of the red one. In this sample, four concentric circles with radiuses of 30, 60, 90 and 120 are adopted. Their radiuses have equal difference of 30. The number of concentric rings and equal difference in radiuses determine the scale of neighborhood area.

 Copyright ⓒ 2016 SERSC

In Figure 1, each circle is equally divided into 12 bins. All the bins are ranked based on the ring they belong to and the anticlockwise angle range they cover. The four circles are sorted in accordance to their radius from small to large. Furthermore, the very first bin starts from right horizontal radius (indicating 0°) in the first circle, and the other 11 bins in the first circle are ranked from 2 to 12 respectively. Accordingly, bins, numbered from 13 to 24, start from right horizontal in the second circle. Totally, there are 48 bins in the four concentric rings, describing relative shapes among the key points within the neighborhood area. Finally, a histogram with 48 bins is generated accordingly. Every bin in the concentric rings is transformed to the corresponding one in the histogram. For example, if a blue key point locates in Bin One, accordingly, the first bin in the histogram would be added by one. The process is repeated on each key point in the image; so that we have a feature of 48 dimensions for each key point (see Figure 2).

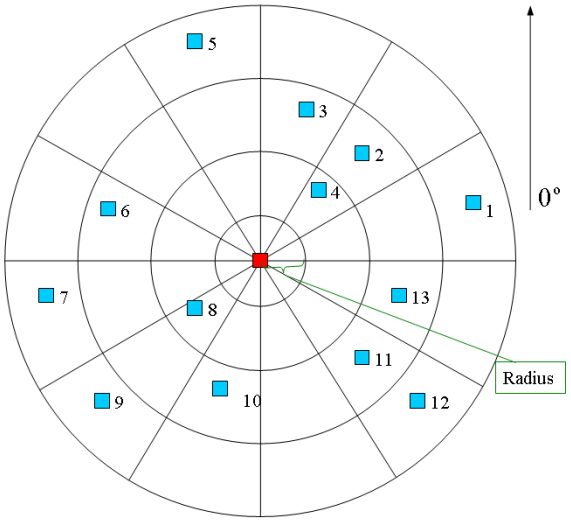

Figure 1. Description of HSD

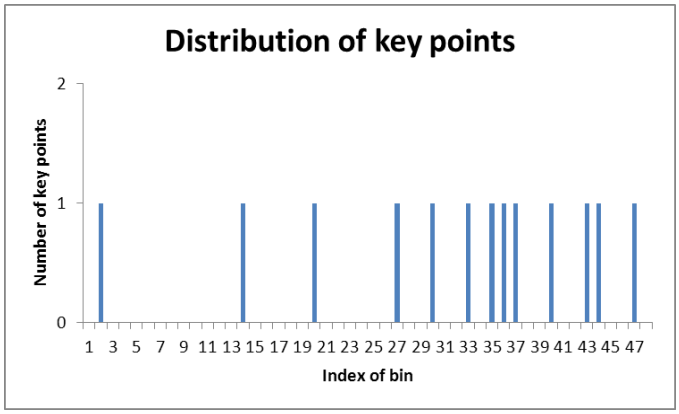

Figure 2. Histogram of Sample Data

4. Experiments

Our experiment is done on the basis of Core-1000 dataset. It has 10 groups and 100 images for each. A variety of categories, such as dinosaurs, buses, landscapes, human beings, are covered. It is one of the standard databases for evaluating the algorithm in image retrieval [36].

Copyright ⓒ 2016 SERSC

4.1 Features for Comparison

To assess the performance of our feature statistically and objectively, SED and TXT are used to be comparative methods. They are briefly introduced as follows:

4.1.1 Structure Elements' Descriptor (*SED*): SED is a novel feature proposed by Wang Xingyuan and Wang Zongyu [36]. It is a shape descriptor of all the pixels by grouping them according to their intensity, as described below:

(1) Transform image from *RGB* color space to *HSV*

(2) Re-assign the intensity value of every pixel in each channel according to their original one in *HSV* color space with the equations (3)-(5):

$$H=\begin{cases} 0, H\in[0,24]\cup[345,360] \\ 1, H\in[25,49] \\ 2, H\in[50,79] \\ 3, H\in[80,159] \\ 4, H\in[160,194] \\ 5, H\in[195,264] \\ 6, H\in[265,284] \\ 7, H\in[285,344] \end{cases} \tag{3}$$

$$S=\begin{cases} 0, S\in[0,0.15] \\ 1, S\in(0.15,0.8] \\ 2, S\in(0.8,1] \end{cases} \tag{4}$$

$$V=\begin{cases} 0, V\in[0,0.15] \\ 1, V\in(0.15,0.8] \\ 2, V\in(0.8,1] \end{cases} \tag{5}$$

(3) Generate a gray image *G* with the re-assigned *H,V* and *S* channels

$$G=9H+3S+V \tag{6}$$

Therefore, *G* is quantized into 72 (8x3x3) bins.

(4) Calculate shape and directions of pixels with the same bin in image *G* by means of matching five structuring elements. Totally, we can have 72x5=360 dimensional feature SED to describe an image.

4.1.2 Texture Characteristics (TXT): Since entropy, mean value and variance are common features to describe the overall distribution of pixels in an image, they have been selected as comparative feature in our experiments. Moreover, they are calculated in a color invariant model, as introduced by Lei, *et. al.* [17].

Numerous researches have been conducted to propose a color invariant feature [10, 11, 17]. Invariant color gradients in Gaussian color space [10, 11] are models depending on incident light source, reflection of the object's surface, illumination and the angels observed. The calculation of invariant color feature can be summarized in three steps.

(1) Calculate three channels *E*, E_{λ} and $E_{\lambda\lambda}$ based on *R*, *G* and *B* with the following equation,

 Copyright ⓒ 2016 SERSC

$$\begin{bmatrix} E(x,y) \\ E_{\lambda}(x,y) \\ E_{\lambda\lambda}(x,y) \end{bmatrix} = \begin{pmatrix} 0.06 & 0.63 & 0.27 \\ 0.30 & 0.04 & -0.35 \\ 0.34 & -0.60 & 0.17 \end{pmatrix} \begin{bmatrix} R \\ G \\ B \end{bmatrix} \tag{7}$$

(2) Figure up two gradient images in directions of horizontal (represented by x) and vertical (represented by y) for each channel of *E*, E_{λ} and $E_{\lambda\lambda}$ respectively.

(3) Finally, the invariant color gradient is generated according to three different conditions of illumination and surface features [10, 11, 17].

a) Condition one is uniform illumination, the invariant color gradient *H* can be calculated with the following equation:

$$H_j = \frac{E_{\lambda\lambda} E_{\lambda j} - E_{\lambda} E_{\lambda\lambda j}}{E_{\lambda}^{\ 2} + E_{\lambda\lambda}^{\ 2}} \tag{8}$$

where *j* signifies the direction of gradient, namely *x* and *y*.

b) The second condition not only requires uniform illumination, but also demands inferior smooth surface. The invariant color gradient *C* is determined as,

$$C_{\lambda j} = \frac{E_{\lambda j} E - E_{\lambda} E_j}{E^2}, \quad C_{\lambda\lambda j} = \frac{E_{\lambda\lambda j} E - E_{\lambda\lambda} E_j}{E^2} \tag{9}$$

c) The last hypothesis is also the one demanding the most. Except for the two assumptions in the second condition, it assumes that the reflecting surface is flat. Calculation of invariant color gradient *W* is as follows,

$$W_j = \frac{E_j}{E}, W_{\lambda j} = \frac{E_{\lambda j}}{E}, W_{\lambda\lambda j} = \frac{E_{\lambda\lambda j}}{E} \tag{10}$$

Based on invariant color gradient image, texture information of entropy, mean value and variance in spectral intensity of all the pixels are calculated. Under such conditions, they can represent images with stronger robustness. Especially, mean values and variances are calculated based on convolution operation of three sizes. They are 3x3, 5x5 and 9x9 respectively.

4.2 Selection of Parameter Values in HSD

There are three parameters to be considered for optimization. An appropriate *P* in Harris detector would detect proper key points to represent an image. The second one is the equal difference among radiuses of concentric circles (*Diff_radius*). It determines the scale of neighboring area to describe the shape, composed of key points. The last one is the number of angle bin (*No_angle_bin*). It determines the level of specificity of describing the shape. The amount of circle bin is not in the consideration of optimization, because it plays the same role with *Diff_radius*, reflecting the scale of neighboring area. To optimize the three parameters, *p* value, *Diff_radius* and *No_angle_bin* are initialized to be 180, 30 and 12 respectively. Moreover, images of dinosaurs, buses and flowers in Core-1000 dataset are selected to determine the optimal values of the three parameters.

In the process of optimization, we adopt Euler distance as an assessment of similarity between query image and all the other ones. A query image is randomly selected from each sort of data. We select fifty images with shorter distances than the others. After that, *Precision* and *Recall* are calculated among the fifty images to help evaluate the performance of the parameter towards the query image. *Precision* is the probability of images, belonging to the sort of the selected one among the fifty images. *Recall* is evaluated by calculating the ratio of images, right classified into fifty images of the

Copyright ⓒ 2016 SERSC

selected sort dataset. Commonly, *precision* and *recall* are used to assess the performance of feature in image retrieval. Higher precision and recall indicate better performance. Nevertheless, *Precision* and *Recall* are not smart always. That is true especially for some extreme circumstances. For example, if we pick out one image with the highest similarity to the query image, and the image belongs to the same sort with the query one, *precision* would be 100%, while *recall* is 0%. Therefore, *F-measure* is adopted as a synthesized parameter to assess the performance of image retrieval. It is calculated with the following equation,

$$F - measure = \frac{(a^2 + 1)P \times R}{a^2(P + R)} \tag{11}$$

where P and R represent *Precision* and *Recall* respectively. a is a tunable coefficient, and it is selected to be 1 here.

Evaluation experiment based on each sort of images would iterate ten times. *F-measure* is calculated every time. Finally, we use average *F-measure* of each sort to represent the performance of each group of values in HSD.

The comparison of experimental results with different P value is shown in Figure 3. We use four potential values for P in our experiment. The other parameters are invariants. From their performances in the three sorts of data, we can see that HSD with p of 180 and 150 perform almost the same. Under such conditions, the average *F-measure* of three sorts of data for each p are calculated, and 180 wins with its average *F-measure* being 0.388283, more than 0.387071 of p being 150. There are two potential reasons for this phenomenon. One is that if p value is too small, the key points would be over-detected. Too much detail would ruin the shape descriptor to some extent. The other reason is that if p is large, the details would not be enough to describe a practical shape of our interest.

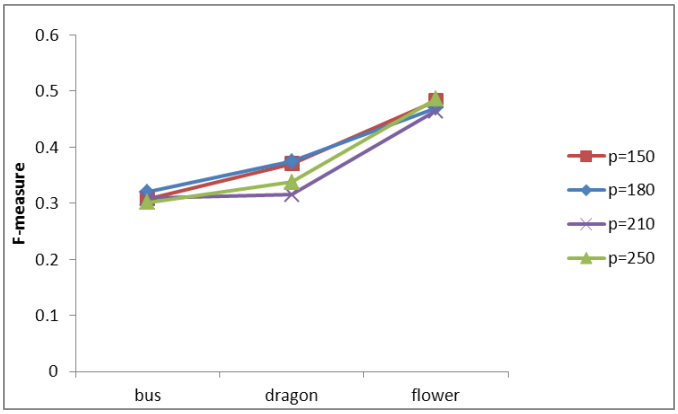

Figure 3. Comparison of Experimental Results with Different *p* Value

In selection of *Diff_radius*, three experimental values are adopted. One is 10 and the other two are 30 and 50 respectively. The experimental results are displayed in Figure 4. Apparently, HSD with *Diff_radius* of 50 achieves the best performance generally in the three sorts of images. That owes to the reason that the neighboring area covered by *Diff_radius* of 50 is larger and the shape can be fully detected, especially for targets with a large size. That exactly explains why *Diff_radius* gets lowest *F-measure* in the sort of flower.

Copyright ⓒ 2016 SERSC

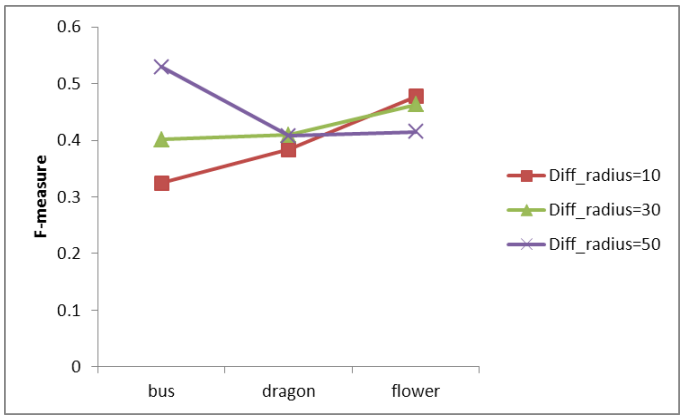

Figure 4. Comparison of Experimental Results of *Diff_Radius*

When it comes to *No_angle_bin*, 8, 12 and 16 are selected to be its potential optimal values. *F-measure*s of each sort of data with each value in *No_angle_bin* are shown in Figure 5. It can be drawn that *No_angle_bin* of 16 and 12 can hardly be discriminated from each other. Again, average *F-measure*s under these two conditions are calculated. Consequently, *No_angle_bin* of 12 wins by increasing 0.000445, compared with *No_angle_bin* of 16. One possible reason for that is that when the number of angle bins is small, HSD would lack details and negatively affect the performance in image retrieval. Another reason for the very close performances of *No_angle_bin* being 12 and 16 is that 12 angle bins have detected enough texture information, dispense with adding 4 more angle bins.

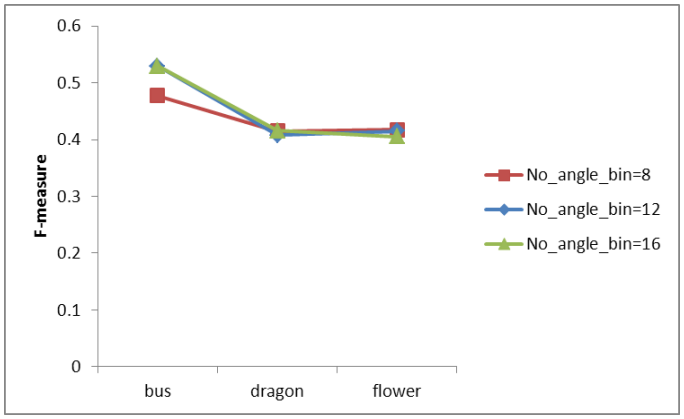

Figure 5. Comparison of Experimental Results with Different Number of No_Angle_Bin

Finally, the parameters in HSD are optimized as follows: p value in key point detector is 180, *Diff_radius* is 50 and *No_angle_bin* is 12. To show our retrieval results by optimized HSD visually, three samples representing three sorts (see Figure 6) and their corresponding fifty retrieved images are listed in Figures 7-9 respectively.

6.1 6.2 6.3

Figure 6. Query Samples of Three Sorts

Copyright ⓒ 2016 SERSC

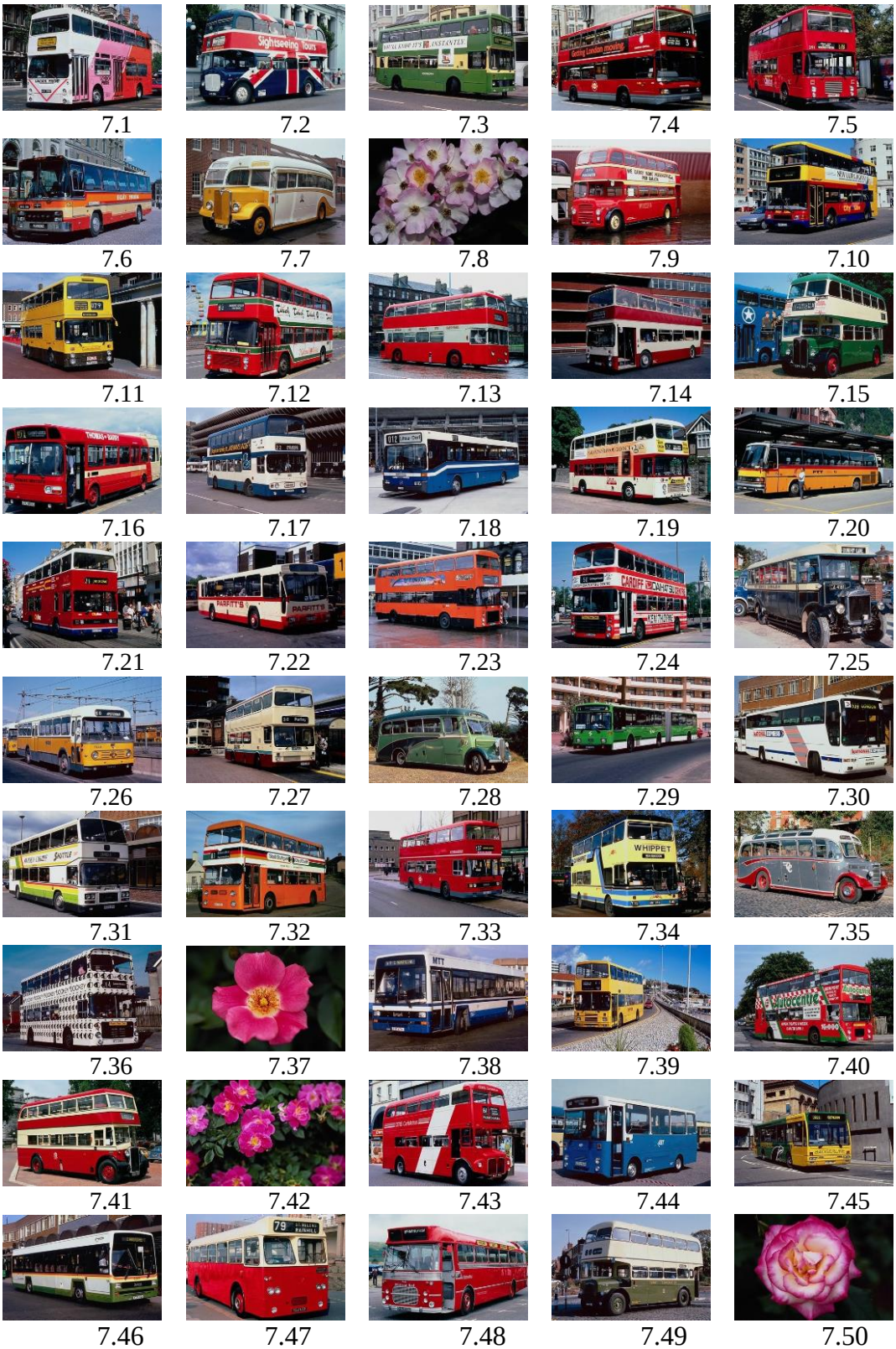

Figure 7. Retrieved Images of Figure 6.1

Among the 50 images in Figure 7, there are 46 images rightly classified and 4 flower images misclassified. HSD performs quite well in retrieving images of bus.

Copyright ⓒ 2016 SERSC

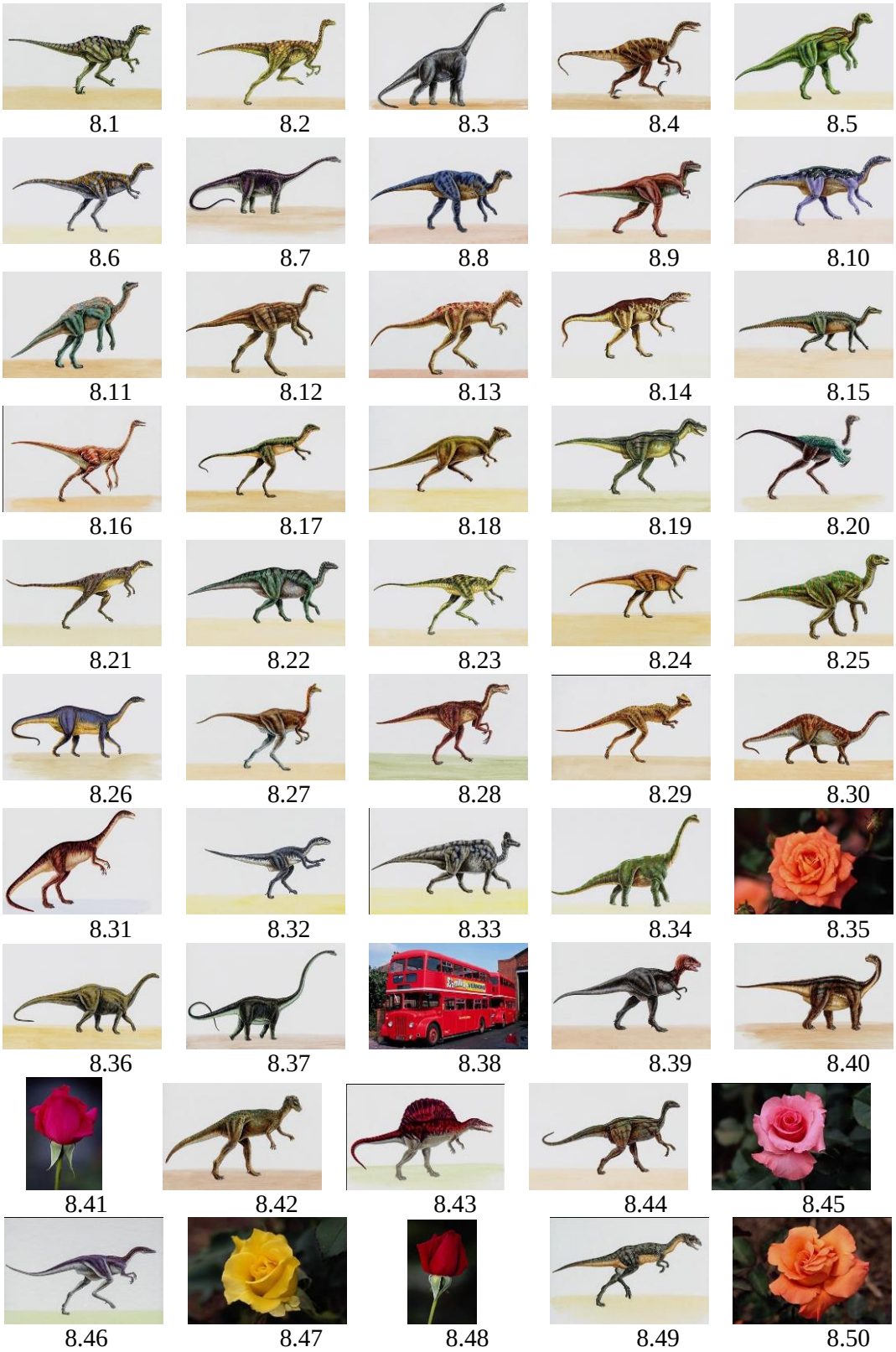

Figure 8. Retrieved Images of Figure 6.2

From Figure 8, we can see that HSD performs well in describing images and easy to be separated within the three sorts. 7 images are misclassified and its precision is pretty high.

Copyright ⓒ 2016 SERSC

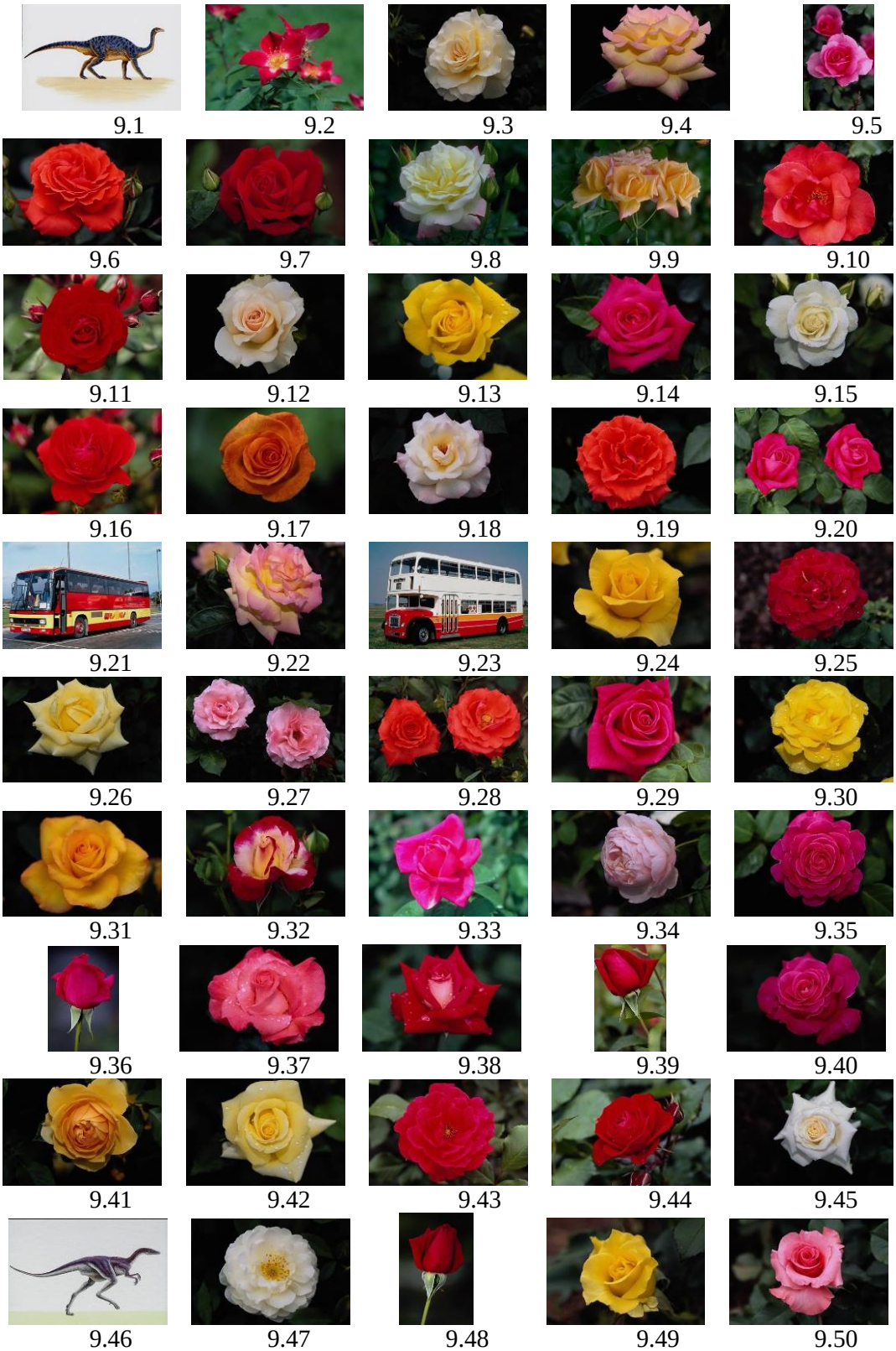

Figure 9. Retrieved Images of Figure 6.3

Figure 9 confirms the robustness of HSD. Of the fifty selected images, only 4 images do not belong to flower. That accurate probability is rather high.

Copyright ⓒ 2016 SERSC

4.3 Experimental Results

With the optimized parameters, all the images in the dataset of Core-1000 are represented by features of HSD, SED and TXT respectively. Average *F-measure* of each sort of data is used to evaluate the performance of each feature. It is calculated by averaging all the *F-measure*s of each retrieved fifty images based on each sample. The experimental results are listed in Figure 10.

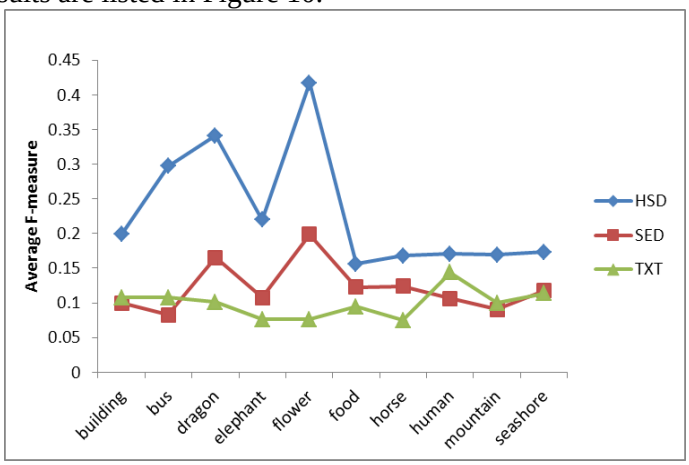

Figure 10. The Comparison of SED, HSD and TXT

From Figure 10 we can see that HSD performs far better than the other two features. Two possible reasons would explain this: one is that HSD describes the relative shape generated by key points only. It is robust with the distribution of our target in the image. However, SED represents shapes of pixels belonging to the sample group, which would be affected by the positions of our target. If only part of the target is in the image or our target exists near to the edge of image, SED would be badly influenced. TXT represents the overall distribution of all the pixels in the image. It is more likely to be affected by the distribution of our target. The other reason is that HSD describes the shape with concentric rings. That would perform details of relative relationships among key points in terms of directions and distances in image. HSD is more flexible, while SED uses five structuring elements with fixed directions to match and TXT takes no directions into consideration.

Conclusion and Discussions

An effective and novel feature is proposed in describing texture feature of an image in this paper. It consists of a new shape descriptor based on the key points detected by Harris detector. The new shape descriptor tells relative connections among key points in concentric circles. HSD is less influenced by the absolute positions of key points in the image, which makes up for the disadvantages of SED and TXT. With concentric rings to formulate the neighboring area of each key point, directions and distances in HSD can be variable compared with five fixed structuring elements in SED. Therefore, HSD shows a better performance compared with SED and TXT using Core-1000 dataset.

Acknowledgments

We sincerely appreciate the generous help from Dr. Juan Xu at Chinese Cooperation in Siemens. It is her supervision and suggestions that help us finish this paper. This research is conducted with the help of the Major State Basic Research Development Program of China (2013CB733405), Major State Basic Research Development Program of China (2010CB950603), Public service sectors (meteorology) Special Fund Research

Copyright ⓒ 2016 SERSC

(GYHY201006042), National Natural Science Foundation of China（41201345）and Major projects of High resolution for earth observation.

References

[1] H.G. Akcay and S. Aksoy, "Automatic Detection of Geospatial Objects Using Multiple Hierarchical Segmentations", Geoscience and Remote Sensing, IEEE Transactions on vol. 46, **(2008)**, pp. 2097-2111.
[2] A. Albiol, D. Monzo, A. Martin, J. Sastre and A. Albiol, "Face recognition using HOG–EBGM", Pattern Recognition Letters, vol. 29, no. 10, **(2008)**, pp. 1537-1543.
[3] S. Banerji, A. Sinha and C. Liu, "New image descriptors based on color, texture, shape, and wavelets for object and scene image classification", Neurocomputing, vol. 117, **(2013)**, pp. 173-185.
[4] T. Celik and T. Tjahjadi, "Bayesian texture classification and retrieval based on multiscale feature vector", Pattern Recognition Letters, vol. 32, no. 2, **(2011)**, pp. 159-167.
[5] J. Chanussot, J. A. Benediktsson and M. Fauvel, "Classification of remote sensing images from urban areas using a fuzzy possibilistic model", Geoscience and Remote Sensing Letters, vol. 3, no. 1, **(2006)**, pp. 40-44.
[6] L. Chen, W. Lu, J. Ni, W. Sun and J. Huang, "Region duplication detection based on Harris corner points and step sector statistics", Journal of Visual Communication and Image Representation, vol. 24, no. 3, **(2013)**, pp. 244-254.
[7] M. Chini, N. Pierdicca and W.J. Emery, "Exploiting SAR and VHR Optical Images to Quantify Damage Caused by the 2003 Bam Earthquake", Geoscience and Remote Sensing, IEEE Transactions on vol. 47, no. 1, **(2009)**, pp. 145-152.
[8] M. Dalla Mura, J. A. Benediktsson, B. Waske and L. Bruzzone, "Morphological Attribute Profiles for the Analysis of Very High Resolution Images", Geoscience and Remote Sensing, IEEE Transactions on vol. 48, no. 10, **(2010)**, pp. 3747-3762.
[9] A. El-ghazal, O. Basir and S. Belkasim, "Invariant curvature-based Fourier shape descriptors", Journal of Visual Communication and Image Representation, vol. 23, no. 4, **(2012)**, pp. 622-633.
[10] J.-M. Geusebroek, R. Boomgaard, A.M. Smeulders and A. Dev, "Color and scale: The spatial structure of color images", Computer Vision - ECCV 2000, Springer Berlin Heidelberg, **(2000)**.
[11] J.M.Geusebroek, R.V.D. Boomgaard, A.W.M. Smeulders and H. Geerts, "Color invariance". Pattern Analysis and Machine Intelligence, IEEE Transactions on, vol. 23, no. 12, **(2001)**, pp. 1338-1350.
[12] L. Gueguen and M. Pesaresi, "Multi scale Harris corner detector based on Differential Morphological Decomposition", Pattern Recognition Letters, vol. 32, no. 14, **(2011)**, pp. 1714-1719.
[13] C. Harris and M. Stephens. "A combined corner and edge detector", In Proceedings of the Fourth Alvey Vision Conference, Manchester, UK, **(1988)**.
[14] R. Hu and J. Collomosse, "A performance evaluation of gradient field HOG descriptor for sketch based image retrieval", Computer Vision and Image Understanding, vol. 117, no.7, **(2013)**, pp. 790-806.
[15] J. Inglada, "Automatic recognition of man-made objects in high resolution optical remote sensing images by SVM classification of geometric image features", ISPRS Journal of Photogrammetry and Remote Sensing, vol. 62, no. 3, **(2007)**, pp. 236-248.
[16] R.M. Lark, "Geostatistical description of texture on an aerial photograph for discriminating classes of land cover", International Journal of Remote Sensing, vol. 17, **(1996)**, pp. 2115-2133.
[17] Z Lei, T. Fang and D. Li, "Histogram of oriented gradient detector with color-invariant gradients in Gaussian color space", Optical Engineering, vol. 49, no. 10, **(2010)**, pp. 109701-109701.
[18] K. Liao, G. Liu and Y. Hui, "An Improvement to the SIFT Descriptor for Image Representation and Matching", Pattern Recognition Letters, vol. 34, no. 11, **(2013)**, pp. 1211-1220.
[19] C.-H. Lin, D.-C. Huang, Y.-K. Chan, K.-H. Chen and Y.-J. Chang, "Fast color-spatial feature based image retrieval methods", Expert Systems with Applications, vol. 38, no. 9, **(2011)**, pp. 11412-11420.
[20] G.-H. Liu, L. Zhang, Y. K. Huo, Z-Y. Li and J.Y. Yu, "Image retrieval based on micro-structure descriptor", Pattern Recognition, vol. 44, no. 9, **(2011)**, pp. 2123-2133.
[21] G.-H. Liu, L. Zhang, Y.-K. Hou, Z.-Y. Li and J.Y. Yang, "Image retrieval based on multi-texton histogram", Pattern Recognition, vol. 43, no. 7, **(2010)**, pp. 2380-2389.
[22] Y. Luo, C.-M. Wu and Y. Zhang, "Facial expression recognition based on fusion feature of PCA and LBP with SVM", Optik-International Journal for Light and Electron Optics, vol. 124, no.17, **(2013)**, pp. 2767-2770.
[23] M. Gouiffès and B. Zavidovique, "Body color sets: A compact and reliable representation of images", Journal of Visual Communication and Image Representation, vol. 22, no. 1, **(2011)**, pp. 48-60.
[24] F. P. Miranda, L. E. N. Fonseca and J. R. Carr, "Semivariogram textural classification of JERS-1(Fuyo-1) SAR data obtained over a flooded area of the Amazon rainforest", International Journal of Remote Sensing, vol. 19, no. 3, **(1998)**, pp. 549-556.
[25] S. Murala, R.P. Maheshwari and R. Balasubramanian, "Local Tetra Patterns: A New Feature Descriptor for Content-Based Image Retrieval", Image Processing, IEEE Transactions on vol. 21, no. 5, **(2012),** pp. 2874-2886.
[26] J. A. Noble, "Finding corners", Image and Vision Computing, vol. 6, no. 2, **(1988)**, pp. 121-128.

 Copyright ⓒ 2016 SERSC

[27] Y. Pang, Y. Yuan, X. Li and J. Pan, "Efficient HOG human detection", Signal Processing, vol. 91, no.4, **(2011)**, pp. 773-781.
[28] G. Quellec, M. Lamard, G. Cazuguel, B. Cochener and C. Roux, "Adaptive Nonseparable Wavelet Transform via Lifting and its Application to Content-Based Image Retrieval", Image Processing, IEEE Transactions on vol. 19, no. 1, pp. 25-35, **(2010)**.
[29] V. F. R.-Galiano, M. C.-Olmo, F. A.-Hernandez, P.M. Atkinson and C. Jeganathan, "Random Forest classification of Mediterranean land cover using multi-seasonal imagery and multi-seasonal texture", Remote Sensing of Environment, vol. 121, **(2012)**, pp. 93-107.
[30] X. Sun, J. Wang, R. Chen, L. Kong and M.F.H. She, "Directional Gaussian Filter-based LBP Descriptor For Textural Image Classification", Procedia Engineering, vol. 15, **(2011)**, pp. 1771-1779.
[31] C. Tan, H. Wang and D. Pei, "SWF-SIFT Approach for Infrared Face Recognition", Tsinghua Science & Technology, vol. 15, no. 3, **(2010)**, pp. 357-362.
[32] P. Tissainayagam and D. Suter, "Assessing the performance of corner detectors for point feature tracking applications", Image and Vision Computing, vol. 22, no. 8, **(2004)**, pp. 663-679.
[33] D.Tuia, F. Pacifici, M. Kanevski and W.J. Emery, "Classification of Very High Spatial Resolution Imagery Using Mathematical Morphology and Support Vector Machines", Geoscience and Remote Sensing, IEEE Transactions on vol. 47, no. 11, **(2009),** pp. 3866-3879.
[34] L. Wang, Z. Niu, C. Wu, R. Xie and H. Huang, "A robust multisource image automatic registration system based on the SIFT descriptor", International Journal of Remote Sensing vol. 33, no. 12, **(2012)**, pp. 3850-3869.
[35] X.Wang and Z. Wang, "A novel method for image retrieval based on structure elements' descriptor", Journal of Visual Communication and Image Representation, vol. 24, no. 1, **(2013)**, pp. 63-74.
[36] X. He, "Laplacian Regularized D-Optimal Design for Active Learning and Its Application to Image Retrieval", Image Processing, IEEE Transactions on vol. 19, no. 1, **(2010),** pp. 254-263.
[37] B. Yang and S. Chen, "A Comparative Study on Local Binary Pattern (LBP) based Face Recognition: LBP Histogram versus LBP Image", Neurocomputing, vol. 120, **(2013)**, pp. 365-379.
[38] K. Zagoris, K. Ergina and N. Papamarkos, "Image retrieval systems based on compact shape descriptor and relevance feedback information", Journal of Visual Communication and Image Representation, vol. 22, no.5, **(2011)**, pp. 378-39.

Authors

Ying Guo received her B. Eng. Degree in automatic control and the M.S. in control engineering both from from Liaoning Shihua University, China, in 2002 and 2012 respectively. She is the Lecturer at School of Information and Control Engineering of Liaoning Shihua University. Her research interests include image processing, predictive control and intelligent instrument design. She has published 4 research papers in this research direction.

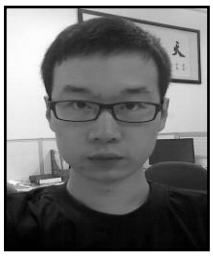

Siquan Yu received his B. Eng. Degree in automatic control and the M.S. in pattern recognition both from from Liaoning Shihua University, China, in 2011 and 2015 respectively. His research is focus on image processing and pattern recognition, hand posture recognition. He has published 2 research papers and 2 patents of invention in this research direction.

 Copyright ⓒ 2016 SERSC